### Title
How Does Antarctic Bottom Water Cross the Southern Ocean?




### Journal
Geophysical Research Letters, 49(7)

### ISSN
0094-8276



### Authors
Solodoch, A
Stewart, AL
Hogg, A McC
et al.



### Publication Date
2022-04-16

### DOI
10.1029/2021gl097211

# How does Antarctic Bottom Water Cross the Southern Ocean?

**A. Solodoch[1], A. L. Stewart[1], A. McC. Hogg [2,3], A. K. Morrison [2,4], A. E. Kiss [2,3], A. F. Thompson [5], S. G. Purkey [6], and L. Cimoli [6]**

[1]Department of Atmospheric and Oceanic Sciences, University of California, Los Angeles, CA, USA
[2]Research School of Earth Sciences, Australian National University, Canberra, Australia
[3]ARC Centre of Excellence for Climate Extremes, Australia
[4]Australian Centre for Excellence in Antarctic Science, Australia
[5]California Institute of Technology, Environmental Science and Engineering, Pasadena, CA, USA
[6]Scripps Institution of Oceanography, UCSD, San Diego, CA, USA

**Key Points:**

- Antarctic Bottom Water (AABW) export pathways across the Southern Ocean are investigated in a high-resolution (0.1°) numerical model.
- Weddell- and Prydz-sourced AABW tracers blend together before crossing the Southern Ocean, as do Ross- and Adelie-sourced AABW tracers.
- Weddell/Prydz-sourced (Ross/Adelie-sourced) AABW tracers primarily supply the Atlantic and Indian Oceans (Pacific Ocean).

Corresponding author: Aviv Solodoch, `asolodoch@atmos.ucla.edu`

**Abstract**

Antarctic Bottom Water (AABW), which fills the global ocean abyss, is derived from dense water that forms in several distinct Antarctic shelf regions. Previous modeling studies have reached conflicting conclusions regarding export pathways of AABW across the Southern Ocean and the degree to which AABW originating from distinct source regions are blended during their export. This study addresses these questions using passive tracer deployments in a 61-year global high-resolution (0.1°) ocean/sea-ice simulation. Two distinct export "conduits" are identified: Weddell Sea- and Prydz Bay-sourced AABW are blended together and exported mainly to the Atlantic and Indian Oceans, while Ross Sea- and Adelie Land-sourced AABW are exported mainly to the Pacific Ocean. Northward transport of each tracer occurs almost exclusively (>90%) within a single conduit. These findings imply that regional changes in AABW production may impact the three-dimensional structure of the global overturning circulation.

## Plain Language Summary

Cooling, ice formation, and mixing near Antarctica create dense ocean waters, known as Antarctic Bottom Water (AABW). Due to their high density, these waters sink and propagate northward to fill the deepest parts of the Southern, Indian, Pacific, and Atlantic Oceans. Hence AABW export has a significant and near-global impact on deep-ocean circulation and the distribution of physical properties (e.g., salinity, temperature, dissolved oxygen). However, AABW transport pathways are only partially understood. Here we investigate the transport pathways of AABW from its four principal formation regions, using a state-of-the-art numerical simulation of Earth's oceans. We find that the export occurs via two distinct pathways ("conduits"). The geographical boundaries between these conduits occur near seafloor ridges, and little AABW exchange occurs across them. Circulation pathways within each conduit blend together AABW formed in two of the four main formation regions, and export them to different oceans. Identification of these pathways elucidates the origin of observed trends in AABW properties, and helps to predict where these changes may propagate in the coming decades.

## 1 Introduction

Antarctic Bottom Water (AABW) is the densest watermass in the global ocean. It is produced by a series of processes, which begins with the creation of Dense Shelf Water (DSW) over Antarctic continental shelves, and culminates with entrainment of Modified Circumpolar Deep Water as the dense waters cascade down the continental margins (Jacobs, 2004). AABW and its lighter derivatives (herein referred to colloquially as AABW - see SI text S3) are exported northward to the Atlantic, Indian, and Pacific Oceans within the abyssal cell of the Meridional Overturning Circulation (MOC) (Talley, 2013). AABW fills 30-40% of the ocean volume (Johnson, 2008), and hence affects stratification, circulation, and mixing rates globally (e.g., see discussion in Zhang et al. (2020)). Moreover, AABW formation and export ventilates the abyssal ocean with dissolved oxygen (Hotinski et al., 2001; Gordon, 2009). Finally, AABW represents a vast reservoir of $CO_2$, which may affect climate significantly over centennial or longer time scales (Skinner et al., 2010; Rae et al., 2018). Despite these global impacts, the pathways of AABW export are not well understood, partially due to the logistical and technological challenges of observing the depths of the remote Southern Ocean.

AABW forms in several distinct coastal sites, which complicates the ability to track the export of a single AABW water mass (Orsi et al., 1999; Jacobs, 2004; Johnson, 2008). The shelf water component of AABW is sourced mainly from water formed in the Ross Sea, Weddell Sea, Prydz Bay, and Adelie Land (Purkey et al., 2018). This study addresses whether these different source waters *blend* within the Southern Ocean, before reaching the northern basins and thus export uniform AABW properties, or if each source feeds different *conduits* northwards across the Southern Ocean, with minimal blending with other AABW source waters. Here we refer to these two limits as "blender" or "conduit" paradigms, respectively, of AABW export from the Southern Ocean. Resolution of whether AABW export is closer to the blender or the conduit limit will provide insight into the ocean's evolution in a warming climate. Trends in AABW properties (salinity, temperature, and thickness) that have been observed in recent decades, are not uniformly distributed spatially. In the Southern Ocean (Purkey et al., 2018), it is not yet possible to determine with confidence which AABW formation regions are responsible for these trends. Likewise, the blender/conduit question has a direct bearing on past (Adkins, 2013) and future evolution of AABW properties, and the time scales over which these changes occur. Finally, improved information about the governing transport processes may help focus observational efforts in locations where the majority of AABW export occurs.

Observational constraints on AABW export pathways are limited (Purkey et al., 2018), and numerical models have produced contrasting results. Van Sebille et al. (2013) calculated offline 500-year particle pathways in the Southern Ocean to track AABW export, using three years of velocity output from an ocean and sea-ice state estimate, the Southern Ocean State Estimate (SOSE) (Mazloff et al., 2010). They found that AABW sources blended together effectively in the Southern Ocean before export to the northern basins, in support of the blender paradigm. In contrast, Kusahara et al. (2017) found little blending of AABW from different source regions in the Southern Ocean. Using a numerical ocean/sea-ice/ice-shelf model, they integrated online for 25-years nine tracers representing different AABW formation regions. Each tracer was associated with different pathways, consistent with strong bathymetric steering.

Here we address the blender vs conduit question over an intermediate, 61-year time scale, using a global ocean and sea-ice model (Kiss et al., 2020) at $\sim$ 2-4 times higher resolution than the aforementioned studies. The model includes online integration of four passive tracers in order to track the four main AABW source waters. The methodology is introduced in section 2. The results (section 3) show that two export "conduits" occur, with horizontal (section 3.1) and vertical (section 3.2) blending between different tracers within, but not between, conduits. We further quantify (section 3.3) the export fractions of each source water to each ocean basin. In section 4 we provide a summary, compare our results to previous studies, and discuss potential implications.

## 2 Methods

We analyze a global ocean and sea-ice simulation, an updated version of the ACCESS-OM2-01 model presented in Kiss et al. (2020), integrated from 1958 to 2018 (the third model forcing cycle, see SI). The model has a horizontal resolution between $\approx$11.5 km near the equator, and 4 km near the Antarctic shelves. Configuration and integration details are given in the SI. Comparison with observations (SI sections S2, S6, and S7) confirms the fidelity of the model AABW-related circulation and properties; additional validation of the recent model version appears in Kiss et al. (2020) and Morrison et al. (2020).

Four passive tracers representing distinct AABW source regions are integrated within the model. Each AABW tracer is linearly restored to a value of 1 in the surface grid cell within its corresponding Antarctic shelf region, and is destroyed at surface grid cells outside of that shelf region (with time scales of 1000 seconds, and 1 day, respectively). Tracers evolve passively in the ocean interior via advection and diffusion. The four shelf regions chosen (figure 1) correspond to those in which observations have confirmed that intense DSW formation occurs: the Weddell Sea, Prydz Bay, Adelie Land, and Ross Sea shelves (Orsi et al., 1999; Purkey et al., 2018). Based on surface buoyancy fluxes (SI text S9, and table S1), these four regions capture about 90% of DSW formation on the Antarctic shelves in the model. Model AABW production rates in each region are given in table S1. We refer to these model tracers as Weddell-, Prydz-, Adelie-, and Ross-sourced AABW. A snapshot of tracer concentration near the seafloor at the end of the model integration period (2018-12-31) is shown in figure 1. Several distinct northward routes are evident from these distributions, as discussed in section 3. In the following analyses we examine the properties and transport of water of density $\sigma_2 \geq 37.125$ kg/m$^3$, since that is approximately the upper bound of northward flow within the Southern Ocean abyssal MOC branch in the model (SI). Unless specified otherwise, presented concentrations are averaged vertically under this isopycnal, and temporally over the last model decade, 2009-2018.

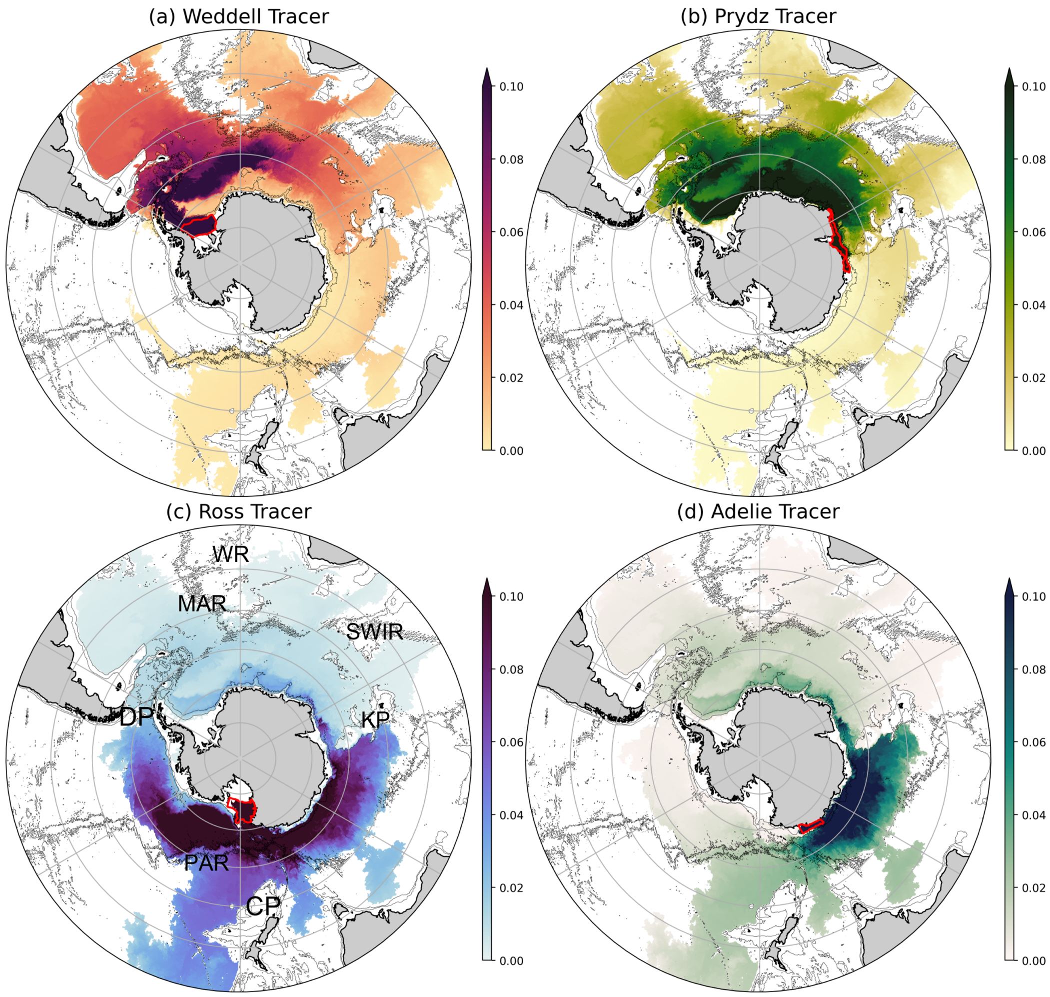


**Figure 1.** Snapshot of AABW tracer concentrations after 61 years of model integration (i.e., at model date 2018-12-31). Tracer concentrations are evaluated at the seafloor-adjacent model cell, in regions where the density $\sigma_2 \geq 37.125$ kg/m$^3$, i.e., within the density range of northward flow of the Southern Ocean abyssal MOC branch: (a) Weddell Sea tracer, (b) Prydz Bay tracer, (c) Ross Sea tracer, (d) Adelie Land tracer. To focus on the principal pathways, tracer values less than 0.001 are not displayed, and the colormap is saturated at concentration 0.1. Tracer source region masks are shown in red in each panel. Gray contours show the 1 and 3-km isobaths. Acronyms in panel (c) denote Drake Passage (DP), the Mid-Atlantic-Ridge (MAR), Walvis Ridge (WR), Southwest Indian Ridge (SWIR), Kerguelen Plateau (KP), Campbell Plateau (CP), and the Pacific-Antarctic Ridge (PAR).

## 3 Results

Export pathways of AABW from the Southern Ocean are visually evident in the tracer distributions in figure 1, as well as in tracer evolution animations (SI). The main export routes occur within broad belts west of the Mid Atlantic Ridge in the Atlantic Ocean; west of the Southwest Indian Ridge, and west of the Kerguelen Plateau in the Indian Ocean; and east of the Campbell Plateau in the Pacific Ocean. Topographic features are identified in figure 1c. Northward AABW export in additional routes is latitudinally limited by bathymetry, e.g., by the Walvis Ridge in the South-East Atlantic (see figure S1, which extends further north). Prior to northward export, Prydz-sourced AABW joins Weddell-sourced AABW via westward advection along the continental slope. Upstream of their northward export to the Pacific, Adelie- and Ross-sourced AABW both populate a wide recirculation between the Pacific-Antarctic Ridge and Kerguelen Plateau (see section 3.1 as well), which in its offshore side advects both tracers eastward towards Campbell Plateau. These pathways are generally consistent with the available observations (Orsi et al., 1999) (SI text S6). In summary, AABW export routes can be differentiated based on AABW origin: Weddell and Prydz AABW are exported together, mainly to the Atlantic and Indian Oceans, while Ross and Adelie AABW are exported mainly to the Pacific Ocean. Hence we identify that the model AABW export routes can be conceptually partitioned to two conduits, with each conduit transporting AABW sourced mainly from two locations, distinct from the other conduit.

### 3.1 Horizontal blending of AABW source waters

To test the degree of blending between tracers, and the locations where the blending ensues, we examine a two-tracer metric ($B(x, y)$, eq. 1, where $x$ and $y$ mark longitude and latitude, respectively), which attains near-zero values when the tracers values differ significantly, and approaches one when the tracer values are similar:

$$B(x, y) = \frac{2A_1A_2}{A_1^2 + A_2^2}. \tag{1}$$

Here $A_1$ and $A_2$ are (2009-2018) time-averaged concentrations of two different tracers within the AABW layer (see section 2). Sharp gradients in $B$ may be interpreted as regions where blending occurs. Following westward advection of Prydz-sourced AABW along the continental slope, this water mass joins and blends with Weddell-sourced AABW near the Weddell Sea southern and western shelf break regions, and possibly in the central Weddell Gyre, as can be seen from the locations of high $B$ gradient in figure 2a. Values close to $B = 1$, indicating almost complete blending, occur everywhere downstream in the northward and eastward pathways (section 3). Ross-sourced AABW blends with Adelie-sourced AABW (figure 2b) as both are advected westward along the continental slope and return in the eastward recirculation (figure 1). However, AABW located east of New Zealand has values of $B$ that are slightly lower than in the recirculation to the west. This suggests that some Ross-sourced AABW is exported directly northward without first recirculating between the Pacific-Antarctic Ridge and the Kerguelen Plateau. Very little Adelie-sourced AABW crosses the Pacific-Antarctic Ridge eastward, and hence this region is dominated by Ross-sourced AABW (see figure 1 as well). Examination of the metric $B$ between all other tracer pairs (SI figure S4) shows very little blending between them.

To complement the local metric $B$ and to test the visually identified pathways, we examine longitudinal correlations $C_{TC}$ between pairs of (2009-2018) time-averaged AABW *tracer concentrations*, as a function of latitude $\phi$:

$$C_{TC}(\phi) = \frac{\langle A_1' A_2' \rangle}{\sqrt{\langle A_1'^2 \rangle \langle A_2'^2 \rangle}}, \tag{2}$$

where angled brackets denote zonal-means, and primes denote deviations from zonal means. This metric measures the similarity between zonal distributions of different tracers. The

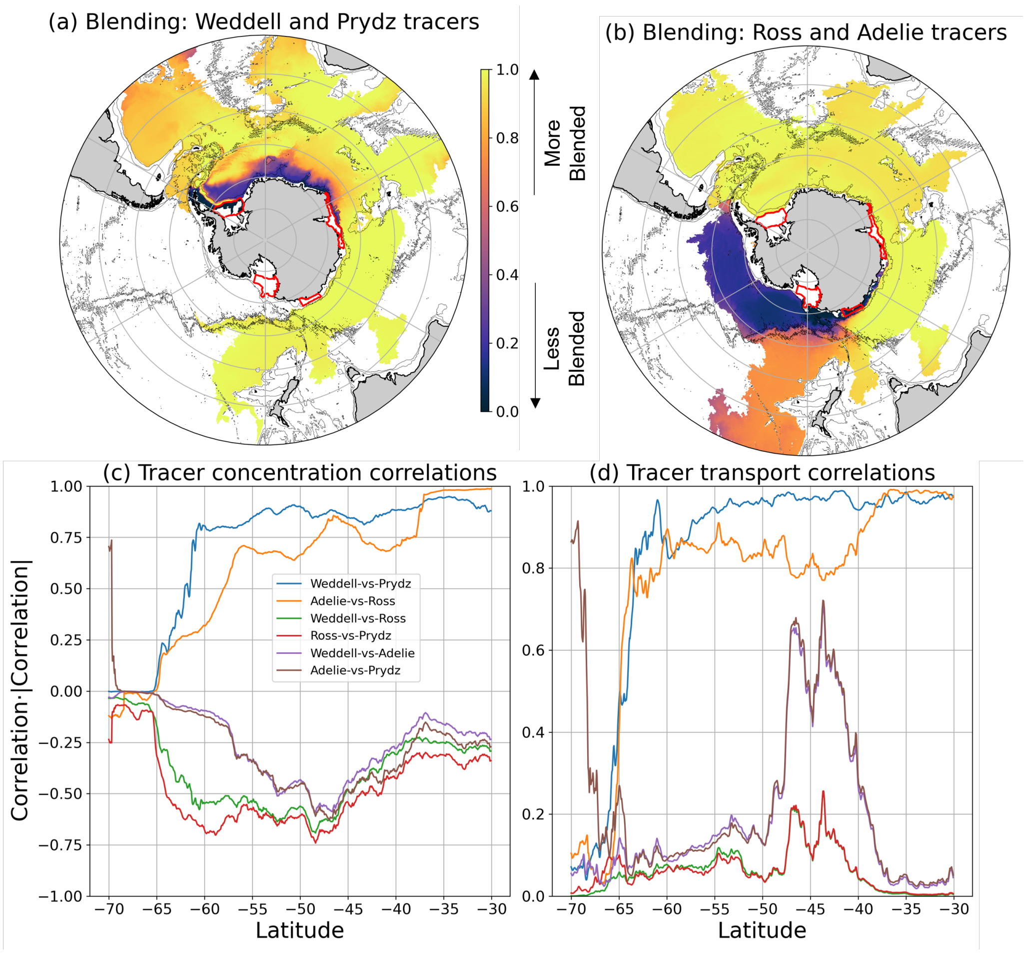


**Figure 2.** The horizontal blending metric $B$ (Eq. (1)) for (a) the Weddell and Prydz tracers and (b) the Ross and Adelie tracers. Tracer values lower than 0.001 are masked. Tracer masks and bathymetry are shown as in figure 1. Zonal-correlation metrics (Eq. (2)) between (c) tracer concentrations and (d) tracer transports, for different tracer pairs. The quantity plotted is $C|C|$, where $C$ is the relevant correlation ($C_{TC}$ or $C_{TT}$). Tracer concentrations and isopycnal transports are evaluated within the AABW layer $\sigma_2 \geq 37.125$ kg/m$^3$, and averaged in time over the last model decade. Note different ordinate ranges are used in panels (c) and (d).

quantity shown in figure 2c is $C_{TC}|C_{TC}|$, which reveals both the magnitude, i.e., the common-variance $C_{TC}^2$, and the correlation sign.

There are high positive correlations $C_{TC}$ between Weddell- and Prydz-sourced AABW, with $C_{TC}^2$ greater than 0.75 north of 60°S (figure 2c), showing they take similar pathways north of this latitude. The correlation between Ross- and Adelie-sourced AABW is positive and similarly high, but at a larger meridional distance from Antarctica ($\approx$ 55°S). In contrast, correlations between tracers from different "conduits", e.g., Weddell vs Ross, are negative, i.e., Weddell AABW concentrations tend to be higher (lower) than average where Ross AABW concentrations are lower (higher) than average, consistent with these AABW varieties having different northward pathways.

To complement the concentration correlations, we quantify zonal correlations between *meridional tracer transports* (SI text S4), $C_{TT}$ (figure 2d). The correlation $C_{TT}$

is calculated according to (2), with tracer transport $F_i$ (defined in SI equation S4) replacing tracer concentration $A_i$. Again, correlations are high within the Weddell-Prydz pair and within the Ross-Adelie pair, with $C^2_{TT} > 0.8$. Tracer transport correlations within other AABW pairs are lower, with $C^2_{TT} < 0.2$ except within a narrow band around 45°S. The higher correlation near 45°S appears to be due to the presence of a large (∼ 20 Sv) recirculation of AABW in the Argentine Basin. The recirculation strength is of similar magnitude to the total abyssal MOC cell in the model and in observations (SI text S2). The Deep Western Boundary Current (DWBC) and the adjacent recirculation cause higher local correlation in transports for all tracer pairs at this latitude. The recirculation is likely the model manifestation of the Zapiola Anticyclone, which in observations has a large-magnitude (∼10cm s$^{-1}$) near-bottom horizontal velocity signature and a 100 Sv total top-to-bottom horizontal transport magnitude (Weatherly, 1993; Saunders & King, 1995). Another narrow correlation peak occurs between Prydz and Adelie tracers around 70°S. Both Prydz and Adelie tracers are formed strictly north of 70°S, and reach further south mainly within the Weddell Sea.

Thus tracer concentration and tracer transport correlations, as well as the blending metric $B$, also support that AABW is exported predominantly within two distinct horizontal pathways or conduits. Longitude-depth tracer distributions (e.g., SI figure S10) are consistent with the horizontal maps shown here, and also show high similarity in the vertical concentration profile of different tracers within each pathway, motivating an examination of tracer-density profiles in the next subsection.

### 3.2 Vertical blending of AABW source waters

In this section we examine the density-profiles of the AABW tracers (figure 3), in order to deduce the degree of vertical blending of AABW tracers with distinct sources that occurs during export. Density-concentration profiles of the identified tracer pairs are more similar to each other than to other tracers. Between Drake Passage and the Kerguelen Plateau (figure 3a), Weddell and Prydz tracers have higher-density centers of mass (are "bottom-heavy") and have order of magnitude higher concentrations than the Ross and Adelie tracers. In contrast, between the Kerguelen Plateau and the Pacific-Antarctic Ridge (figure 3b), the Ross and Adelie tracers are the more bottom-heavy and abundant pair. Between the Pacific-Antarctic Ridge and Drake Passage (figure 3c), the Ross tracer dominates, while other tracers have lower concentrations and peak at lower densities, consistent with figure 2b. The lighter densities and lower concentrations reflect either more mixing along (longer) pathways to a region, or inefficient transport of denser water across the basin topographic boundaries (e.g., Princess Elizabeth Trough south of Kerguelen Plateau, or the Pacific-Antarctic Ridge).

The tracer-density distributions become more similar at greater meridional distances from their formation regions ((figure 3) panels d-f), especially for the identified tracer pairs: the density-profile shapes of the Weddell-Prydz or the Ross-Adelie tracer pair become virtually indistinguishable at 30°S. The growing similarities in vertical profiles suggest a statistical similarity in the histories of vertical mixing within each conduit. These results are consistent with vertical homogenization of AABW sourced from different shelf regions within individual conduits, but relatively little vertical homogenization elsewhere.

### 3.3 Connectivity between AABW shelf sources and ocean basins

Model tracer distributions (sections 3 and 3.2) show that different Antarctic source regions can have very different distributions of AABW export to northward basins. Here we quantitatively assess the connectivity (figure 4) between the AABW tracer source regions and destination regions (the Atlantic, Indian, and Pacific oceans), via a connectivity matrix methodology, after Van Sebille et al. (2013). For each tracer we compute the partitioning of the total northward transport, occurring at 30°S, between the differ-

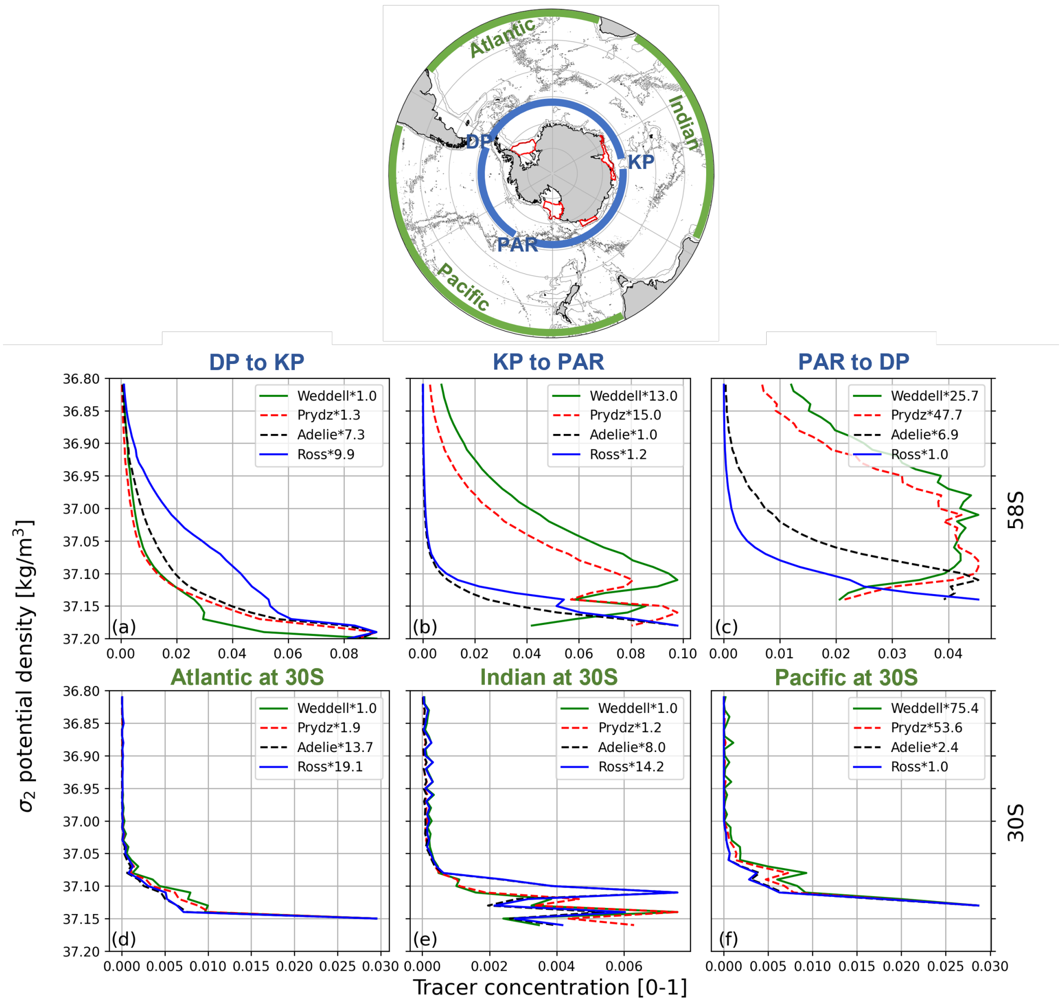


**Figure 3.** Tracer concentration profiles in density space, averaged across 0.5 degree of latitude, and across the longitude range of individual ocean basins: (a-c) 58°S segments between Drake passage (DP), Kerguelen Plateau (KP), and the Pacific-Antarctic Ridge (PAR); (d-f) Atlantic, Indian, and Pacific Oceans at 30°S. To highlight vertical structure rather than peak values, each profile is multiplied by a constant factor (given in each panel) such that its maximal value is identical to that of the tracer with largest maximum in the same region. Segments a-f locations (exact longitudes given in the SI, text S5) are shown in the top panel, along with the tracer masks.

ent ocean basins ("export", green-colored pie charts). Additionally, for each ocean basin (Atlantic, Indian, or Pacific), we compute the relative contribution of the total northward tracer transport, occurring at 30°S, from different individual tracers ("import", red-colored pie charts). Tracer transports within the AABW layer (calculated as explained in SI section 4) are integrated zonally within each basin.

We now quantify the degree to which model AABW pathways through the Southern Ocean can be grouped into two pairs, i.e., conduits. Total AABW tracer "import" (volume flux, reddish pie charts) to the Atlantic and Indian Oceans is dominated by Weddell (58%) and Prydz (34%) AABW tracers. In contrast, import into the Pacific is dominated by Ross (68%) and Adelie (30%) AABW tracers. Export (greenish pie charts) of

Weddell AABW and of Prydz AABW is principally into the Atlantic Ocean, with a secondary export contribution to the Indian Ocean, and a very small fraction (3 and 6 %, respectively) into the Pacific Ocean. Exports of Ross AABW and Adelie AABW are similar to each other and different from the Weddell-Prydz pair, with over 90% exported into the Pacific, and less than 2% into the Atlantic. Total export and import fractions, summed over all source regions or destination basins, respectively, are shown in the insets of figure 4. The largest AABW tracer import is from the Ross Sea (40%), with other areas contributing fractions close to 20% each. Total export is mainly to the Pacific Ocean (57%), and secondarily to the Atlantic Ocean (37%), with only 5% reaching the Indian at 30°S.

## 4 Summary and discussion

Based on a high-resolution numerical model analysis, we show that the export of AABW through the Southern Ocean is accomplished via a combination of the blender and conduit paradigms (Van Sebille et al., 2013; Kusahara et al., 2017). AABW export pathways are guided by prominent topographic features, and manifest in some regions as DWBCs, or by flow through topographic gaps in rift zones (figures 1 and 2(a-b)). Two separate conduits are identified, which are separated by Drake Passage on one side, and by Kerguelen Plateau on the other side. However, AABW formed at different regions that lie along the same conduit route are blended and exported together. Specifically, AABW formed in Prydz Bay travels westward along the continental margin, and joins the northward pathways taken by the AABW formed in the Weddell Sea, i.e., principally along the Scotia Arc, or through gaps in it, into the Atlantic Ocean. Smaller fractions of the Weddell-Prydz pair are recirculated eastwards from the Weddell Sea, and exported into the East Atlantic and the West Indian Ocean. Observational studies indeed suggest that a significant fraction of AABW in the Weddell Sea is sourced from east of the Weddell basin, possibly from the Prydz Bay region (Meredith et al., 2000; Hoppema et al., 2001; Jullion et al., 2014). In contrast to the Weddell-Prydz pair, AABW formed in Adelie Land and in the Ross Sea are exported mainly into the Pacific Ocean. This export occurs principally east of the Campbell Plateau, either after recirculation in the Australian-Antarctic Basin, or through a more direct path northwards for some Ross-sourced AABW water. Observations of AABW in the Australian-Antarctic Basin suggest it is composed of similar fractions of AABW formed in Adelie Land and in the Ross Sea (Thomas et al., 2020).

The numerical configuration used here has several limitations. The horizontal resolution is not sufficient to resolve the Rossby radius of deformation near the Antarctic continental shelves, which may suppress instabilities and lateral mixing. However, AABW tracer distributions and model circulation patterns, including DWBCs, generally compare favourably with observations, supporting the deep pathway interpretations presented in this study (SI text S6). Several biases are identified, including that DWBC volume fluxes are lower than observed in some cases, and that AABW transport into the Indian Ocean is on the low end of predictions from inverse models (SI text S2). The Antarctic Circumpolar Current (ACC) zonal transport and the magnitude of Southern Ocean surface eddy kinetic energy (EKE) are lower than in observations, by ~15% and 40%, respectively. In the future it would be useful to assess the degree to which model biases in ACC zonal transport and in upper ocean EKE affect the AABW pathways, blending, and vertical mixing. Additionally, an ice-shelf model is not employed, and hence Ice Shelf Water is not formed in the model, which may impact AABW formation rates. However, using an ocean/sea-ice/ice-shelf coupled model, Kusahara et al. (2017) found AABW export pathways those presented here.

Kusahara et al. (2017) performed a 25-year online integration of nine different AABW-like tracers initialized in different Antarctic continental shelf regions, and found each tracer was exported across the Southern Ocean in different pathways, consistent with topographic

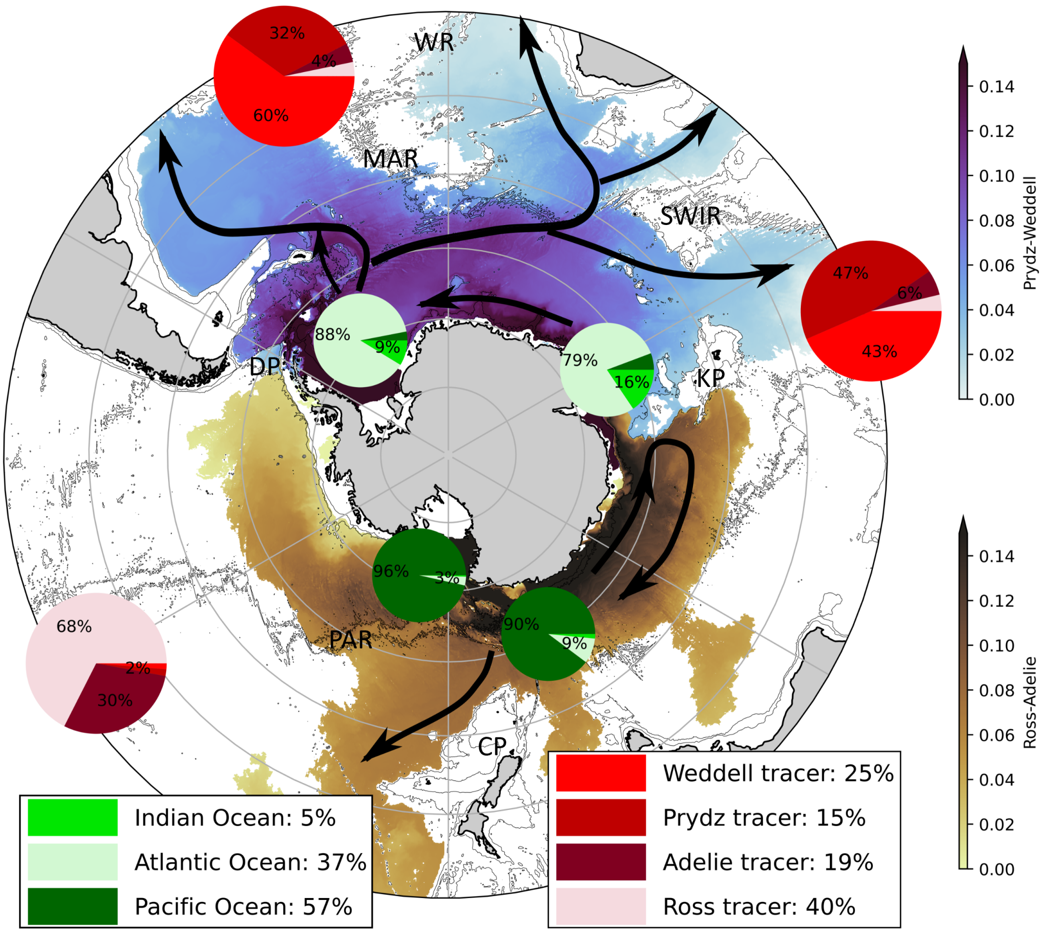


**Figure 4.** Pie charts showing connectivity between the four AABW source regions and each of the three northern basins. For each source region, a green-colored pie chart shows the distribution of its tracer transport northward into different ocean basins at 30°S (Atlantic, Pacific, and Indian). For each ocean basin at 30°S, a red-colored pie chart shows the percentage of northward tracer transport arriving from each source region. Percentages are rounded and appear with greater precision in tables S2-S3. To avoid visual clutter, the smallest percentage in each pie chart is not displayed. The left (right) inset shows the percentages of all tracer transports arriving into individual ocean basins (from individual formation regions). The blue (brown) shading shows the sum of concentrations of Weddell and Prydz (Ross and Adelie) tracers in the AABW layer. The greater of the two sums is shown at each point. Arrows show schematically the AABW export pathways, based on figures 1-2. Acronyms are as in figure 1.

steering. In fact, a close comparison with the tracer maps in Kusahara et al. (2017) suggests that these different routes do merge, or are in the process of merging over time, largely in accordance to the present findings, i.e., to the same two conduits. We also note that the simulated transient tracer (CFC-11) distribution in a 0.1 degree resolution model by Sasai et al. (2004) is consistent with the results that the Kerguelen Plateau is a dividing line across which there is relatively little exchange of AABW.

In contrast to the present results, Van Sebille et al. (2013) found that over a 500-year particle tracking period, AABW formed in different Antarctic regions is blended so effectively as to appear in almost the same proportions in all basins north of the Southern Ocean. A possible bias which may have affected the degree of blending in Van Sebille et al. (2013) was that particles were advected using model velocities recycled every 3 years. Particles could change their densities abruptly at cycle transitions due to a drift in Southern Ocean AABW densities (Mazloff et al., 2010). We also note that AABW particle formation in Van Sebille et al. (2013) appears to have occurred in the open ocean in addition to the Antarctic shelves. The presented connectivity matrix (figure 4) is not directly comparable with that in Van Sebille et al. (2013), due to the shorter time scale considered here: 61 years. In Van Sebille et al. (2013), only $\sim$18% of the particles were exported past 31°S within the first 60 years, but in the present model a decrease in the rate of change of tracer export fluxes in the last model decades (SI figure S2) suggests that AABW pathways and blending may not change drastically over longer time scales. However, it is not possible to distinguish this decrease from interdecadal oscillations with confidence. Diagnosing centennial scale AABW-pathways from a high-resolution model is computationally expensive, and remains to be addressed.

The present investigation of AABW export pathways over decadal time scales is similar to the time scale over which anthropogenic climate change has occurred. Over the last few decades AABW has generally warmed, freshened, and decreased in thickness (Purkey et al., 2018). AABW thickness and salinity trends in the Southern Ocean have spatial patterns that are similar to the model tracer distributions in figure 4: large relative differences in freshening occur across the Kerguelen Plateau, with relatively smaller variations within the regions to each west or east. Likewise, differences in the decrease of AABW thickness between the regions north of Adelie Land and north of the Ross Sea are less than 20%, while the average of the decrease in AABW thickness in these two regions is 50% higher compared with the regions west of Kerguelen Plateau. This suggests that the spatial pattern of AABW property changes may be explained by advection of source water changes along the conduits identified in the present study, and that these changes may propagate in coming decades further downstream along the model conduits identified here, e.g., changes in Prydz-sourced AABW may affect water masses mainly in the Atlantic Ocean. It remains to be seen how such downstream changes in AABW properties would influence the global three dimensional overturning circulation in return. A monitoring system for Southern Ocean AABW export is presently not available other than in the Atlantic sector (Kersale et al., 2020), unlike the situation for North Atlantic Deep Water export for example (McCarthy et al., 2020). However, the identified pathways suggest that it may be sufficient to monitor AABW export at several limited sections along the western regions of the Atlantic, Indian, and Pacific Antarctic sectors.

In summary, we analyze results from a high-resolution model to clarify the multidecadal pathways and blending of AABW in the Southern Ocean, and show that AABW from each of the four main source regions is exported principally in one of two conduits. Weddell- and Prydz-sourced AABW are exported mainly to the Atlantic and Indian Oceans, while Ross- and Adelie-sourced AABW are exported mainly to the Pacific ocean. Knowledge of the connectivity patterns will aid in the attribution of trends in AABW properties to specific source regions, and for understanding of the future evolution of the global AABW distribution. These results therefore have wide implications, given the impact of AABW on global stratification and circulation patterns (Johnson, 2008; Zhang et al., 2020), paleoclimate (Skinner et al., 2010; Rae et al., 2018), and ocean biogeochemistry (Hotinski et al., 2001; Gordon, 2009).

**Acknowledgments**

We thank two anonymous reviewers, which have provided helpful feedback and advice. We also kindly thank Fukamachi Yasushi, of the Institute of Low Temperature Science, Hokkaido University, for sharing their observational data of velocity and temperature

at the Kerguelen Plateau (Fukamachi et al., 2010) (compared with model data in SI text S6).

This work depended on the COSIMA consortium (www.cosima.org.au) which provides the ACCESS-OM2 suite of models. The numerical simulations and analyses were performed with the resources of the National Computational Infrastructure (Canberra, Australia), which is supported by the Australian Government. AS and ALS were partially supported by the National Science Foundation (NSF) under Grant Number OPP-2023244, and by the National Aeronautics and Space Administration ROSES Physical Oceanography program under grant number 80NSSC19K1192. AKM was supported by the Australian Research Council (ARC) DECRA Fellowship DE170100184. AEK was funded by ARC grant LP160100073 and the Australian Government's Australian Antarctic Science Grant Program. AFT was partially supported by NSF grant OCE-2023259.

## Open Research

The model source code is available from `https://github.com/COSIMA/access-om2` and model configuration files are available from `https://github.com/COSIMA/01deg_jra55_iaf/tree/01deg_jra55v140_iaf_cycle3`. Output data is publicly available from `http://dx.doi.org/10.25914/608097cb3433f`.

Reprocessed altimetric sea surface height data (SEALEVEL_GLO_PHY_L4_REP_OBSERVATIONS_008_047) distributed by Copernicus Marine Service (https://resources.marine.copernicus.eu/products) was used in model validation as well, as was data from the World Ocean Data (Locarnini et al., 2018; Zweng et al., 2019) (SI text S6).

## References

Adkins, J. F. (2013). The role of deep ocean circulation in setting glacial climates. *Paleoceanography*, *28*(3), 539–561.

Fukamachi, Y., Rintoul, S., Church, J., Aoki, S., Sokolov, S., Rosenberg, M., & Wakatsuchi, M. (2010). Strong export of Antarctic Bottom Water east of the Kerguelen plateau. *Nature Geoscience*, *3*(5), 327–331.

Gordon, A. L. (2009). Bottom water formation. *Ocean Currents*, *263*, 269.

Hoppema, M., Klatt, O., Roether, W., Fahrbach, E., Bulsiewicz, K., Rodehacke, C., & Rohardt, G. (2001). Prominent renewal of Weddell Sea Deep Water from a remote source. *Journal of Marine Research*, *59*(2), 257–279.

Hotinski, R. M., Bice, K. L., Kump, L. R., Najjar, R. G., & Arthur, M. A. (2001). Ocean stagnation and end-Permian anoxia. *Geology*, *29*(1), 7–10.

Jacobs, S. S. (2004). Bottom water production and its links with the thermohaline circulation. *Antarctic Science*, *16*(4), 427–437.

Johnson, G. C. (2008). Quantifying Antarctic bottom water and North Atlantic deep water volumes. *Journal of Geophysical Research: Oceans*, *113*(C5).

Jullion, L., Garabato, A. C. N., Bacon, S., Meredith, M. P., Brown, P. J., Torres-Valdés, S., … others (2014). The contribution of the Weddell Gyre to the lower limb of the Global Overturning Circulation. *Journal of Geophysical Research: Oceans*, *119*(6), 3357–3377.

Kersale, M., Meinen, C. S., Perez, R. C., Le Henaff, M., Valla, D., Lamont, T., … others (2020). Highly variable upper and abyssal overturning cells in the south atlantic. *Science advances*, *6*(32), eaba7573.

Kiss, A. E., Hogg, A. M., Hannah, N., Boeira Dias, F., Brassington, G. B., Chamberlain, M. A., … others (2020). ACCESS-OM2 v1. 0: A global ocean–sea ice model at three resolutions. *Geoscientific Model Development*, *13*(2), 401–442.

Kusahara, K., Williams, G. D., Tamura, T., Massom, R., & Hasumi, H. (2017). Dense shelf water spreading from Antarctic coastal polynyas to the deep

Southern Ocean: A regional circumpolar model study. *Journal of Geophysical Research: Oceans*, *122*(8), 6238–6253.

Locarnini, M., Mishonov, A., Baranova, O., Boyer, T., Zweng, M., Garcia, H., ... others (2018). World ocean atlas 2018, volume 1: Temperature.

Mazloff, M. R., Heimbach, P., & Wunsch, C. (2010). An eddy-permitting Southern Ocean state estimate. *Journal of Physical Oceanography*, *40*(5), 880–899.

McCarthy, G. D., Brown, P. J., Flagg, C. N., Goni, G., Houpert, L., Hughes, C. W., ... others (2020). Sustainable observations of the AMOC: Methodology and technology. *Reviews of Geophysics*, *58*(1), e2019RG000654.

Meredith, M. P., Locarnini, R. A., Van Scoy, K. A., Watson, A. J., Heywood, K. J., & King, B. A. (2000). On the sources of Weddell Gyre Antarctic Bottom Water. *Journal of Geophysical Research: Oceans*, *105*(C1), 1093–1104.

Morrison, A., Hogg, A. M., England, M. H., & Spence, P. (2020). Warm Circumpolar Deep Water transport toward Antarctica driven by local dense water export in canyons. *Science advances*, *6*(18), eaav2516.

Orsi, A. H., Johnson, G. C., & Bullister, J. L. (1999). Circulation, mixing, and production of Antarctic Bottom Water. *Progress in Oceanography*, *43*(1), 55–109.

Purkey, S. G., Smethie Jr, W. M., Gebbie, G., Gordon, A. L., Sonnerup, R. E., Warner, M. J., & Bullister, J. L. (2018). A synoptic view of the ventilation and circulation of Antarctic Bottom Water from chlorofluorocarbons and natural tracers. *Annual review of marine science*, *10*, 503–527.

Rae, J. W., Burke, A., Robinson, L., Adkins, J. F., Chen, T., Cole, C., ... others (2018). CO2 storage and release in the deep Southern Ocean on millennial to centennial timescales. *Nature*, *562*(7728), 569–573.

Sasai, Y., Ishida, A., Yamanaka, Y., & Sasaki, H. (2004). Chlorofluorocarbons in a global ocean eddy-resolving OGCM: Pathway and formation of Antarctic Bottom Water. *Geophysical research letters*, *31*(12).

Saunders, P. M., & King, B. A. (1995). Bottom currents derived from a shipborne adcp on woce cruise a11 in the south atlantic. *Journal of Physical Oceanography*, *25*(3), 329–347.

Skinner, L. C., Fallon, S., Waelbroeck, C., Michel, E., & Barker, S. (2010). Ventilation of the deep Southern Ocean and deglacial CO2 rise. *Science*, *328*(5982), 1147–1151.

Talley, L. D. (2013). Closure of the global overturning circulation through the Indian, Pacific, and Southern Oceans: Schematics and transports. *Oceanography*, *26*(1), 80–97.

Thomas, G., Purkey, S. G., Roemmich, D., Foppert, A., & Rintoul, S. R. (2020). Spatial Variability of Antarctic Bottom Water in the Australian Antarctic Basin From 2018–2020 Captured by Deep Argo. *Geophysical Research Letters*, *47*(23), e2020GL089467.

Van Sebille, E., Spence, P., Mazloff, M. R., England, M. H., Rintoul, S. R., & Saenko, O. A. (2013). Abyssal connections of Antarctic Bottom Water in a Southern Ocean state estimate. *Geophysical Research Letters*, *40*(10), 2177–2182.

Weatherly, G. L. (1993). On deep-current and hydrographic observations from a mudwave region and elsewhere in the Argentine Basin. *Deep Sea Research Part II: Topical Studies in Oceanography*, *40*(4-5), 939–961.

Zhang, H. J., Whalen, C., Kumar, N., & Purkey, S. G. (2020). Abyssal Stratification Change in the Southwest Pacific Basin.

Zweng, M., Seidov, D., Boyer, T., Locarnini, M., Garcia, H., Mishonov, A., ... others (2019). World ocean atlas 2018, volume 2: Salinity.

## Supporting References

This section lists the SI references which do not appear in the references above.

Abernathey, R. P., Cerovecki, I., Holland, P. R., Newsom, E., Mazloff, M., Talley, L. D. (2016). Water-mass transformation by sea ice in the upper branch of the Southern Ocean overturning. *Nature Geoscience*, 9 (8), 596–601.

Abrahamsen, E. P., Meijers, A. J., Polzin, K. L., Garabato, A. C. N., King, B. A., Firing, Y. L., . . . others (2019). Stabilization of dense Antarctic water supply to the Atlantic Ocean overturning circulation. *Nature Climate Change*, 9 (10), 742–746.

Cessi, P. (2019). The global overturning circulation. *Annual review of marine science*, 11 , 249–270.

De Lavergne, C., Madec, G., Le Sommer, J., Nurser, A. G., Naveira Garabato, A. C. (2016). On the consumption of Antarctic Bottom Water in the abyssal ocean. *Journal of Physical Oceanography*, 46 (2), 635–661.

Donohue, K., Tracey, K., Watts, D., Chidichimo, M. P., Chereskin, T. (2016). Mean antarctic circumpolar current transport measured in drake passage. *Geophysical Research Letters*, 43 (22), 11–760.

Dotto, T. S., Naveira Garabato, A., Bacon, S., Tsamados, M., Holland, P. R., Hooley, J., . . . Meredith, M. P. (2018). Variability of the Ross Gyre, Southern Ocean: drivers and responses revealed by satellite altimetry. *Geophysical Research Letters*, 45 (12), 6195–6204

Fukamachi, Y., Rintoul, S., Church, J., Aoki, S., Sokolov, S., Rosenberg, M., Wakasuchi, M. (2010). Strong export of Antarctic Bottom Water east of the Kerguelen plateau. *Nature Geoscience*, 3 (5), 327–331.

Ganachaud, A., Wunsch, C. (2000). Improved estimates of global ocean circulation, heat transport and mixing from hydrographic data. *Nature*, 408 (6811), 453–457.

Gebbie, G., Huybers, P. (2011). How is the ocean filled? *Geophysical Research Letters*, 38 (6).

Gebbie, G., Huybers, P. (2012). The mean age of ocean waters inferred from radiocarbon observations: Sensitivity to surface sources and accounting for mixing histories. *Journal of Physical Oceanography*, 42 (2), 291–305

Jackett, D. R., McDougall, T. J. (1997). A neutral density variable for the world's oceans. *Journal of Physical Oceanography*, 27 (2), 237–263.

Jackett, D. R., McDougall, T. J., Feistel, R., Wright, D. G., Griffies, S. M. (2006). Algorithms for density, potential temperature, conservative temperature, and the freezing temperature of seawater. *Journal of Atmospheric and Oceanic Technology*, 23 (12), 1709–1728.

Johnson, G. C. (2008). Quantifying Antarctic bottom water and North Atlantic deep water volumes. *Journal of Geophysical Research: Oceans*, 113 (C5).

Johnson, G. C., Purkey, S. G., Toole, J. M. (2008). Reduced Antarctic meridional overturning circulation reaches the North Atlantic Ocean. *Geophysical Research Letters*, 35 (22).

Kunze, E. (2017). The internal-wave-driven meridional overturning circulation. *Journal of Physical Oceanography*, 47 (11), 2673–2689.

Large, W. G., Yeager, S. G. (2009). The global climatology of an interannually varying air–sea flux data set. *Climate dynamics*, 33 (2-3), 341–364.

Lele, R., Purkey, S. G., Nash, J. D., MacKinnon, J. A., Thurnherr, A. M., Whalen, C. B., . . . Talley, L. D. (2021). Abyssal Heat Budget in the Southwest Pacific Basin. *Journal of Physical Oceanography.*

Locarnini, R. A., Mishonov, A. V., Antonov, J. I., Boyer, T. P., Garcia, H. E., Baranova, O. K., . . . Seidov, D. (2013). *World Ocean Atlas 2013*, Volume 1: Temperature (NOAA Atlas NESDIS No. 73). Retrieved from https://data.nodc.noaa.gov/woa/WOA13/DOC/woa13vol1.pdf

Lumpkin, R., Speer, K. (2007). Global ocean meridional overturning. *Journal of Physical Oceanography*, 37 (10), 2550–2562.

Naveira Garabato, A. C., McDonagh, E. L., Stevens, D. P., Heywood, K. J., Sanders, R. J. (2002). On the export of Antarctic bottom water from the Weddell Sea. *Deep Sea Research Part II: Topical Studies in Oceanography*, 49 (21), 4715–4742.

Neme, J., England, M. H., Hogg, A. M. (2021). Seasonal and Interannual Variability of the Weddell Gyre From a High-Resolution Global Ocean-Sea Ice Simulation During 1958–2018. *Journal of Geophysical Research: Oceans*, 126 (11), e2021JC017662.

Reeve, K. A., Boebel, O., Strass, V., Kanzow, T., Gerdes, R. (2019). Horizontal circulation and volume transports in the Weddell Gyre derived from Argo float data. *Progress in Oceanography*, 175 , 263–283.

Reid, J. L. (1986). On the total geostrophic circulation of the South Pacific Ocean: Flow patterns, tracers and transports. *Progress in Oceanography*, 16 (1), 1–61.

Talley, L. D. (2008). Freshwater transport estimates and the global overturning circulation: Shallow, deep and throughflow components. *Progress in Oceanography*, 78 (4), 257–303

Tsujino, H., Urakawa, S., Nakano, H., Small, R. J., Kim, W. M., Yeager, S. G., . . . others (2018). JRA-55 based surface dataset for driving ocean–sea-ice models (JRA55-do). *Ocean Modelling*, 130 , 79–139.

Valla, D., Piola, A. R., Meinen, C. S., Campos, E. (2019). Abyssal transport variations in the southwest South Atlantic: First insights from a long-term observation array at 34.5 S. *Geophysical Research Letters*, 46 (12), 6699–6705.

Whitworth III, T., Nowlin Jr, W. D., Pillsbury, R. D., Moore, M. I., Weiss, R. F. (1991). Observations of the Antarctic Circumpolar Current and deep boundary current in the southwest Atlantic. *Journal of Geophysical Research: Oceans*, 96 (C8), 15105–15118.

Xu, X., Chassignet, E. P., Firing, Y. L., Donohue, K. (2020). Antarctic Circumpolar Current transport through Drake Passage: What can we learn from comparing highresolution model results to observations? *Journal of Geophysical Research: Oceans*, 125 (7), e2020JC016365.

Zweng, M., Reagan, J., Antonov, J., Locarnini, R., Mishonov, A., Boyer, T., . . . Biddle, M. (2013). *World ocean atlas 2013*, volume 2: Salinity. NOAA Atlas NESDIS 74 .